



Constraining the contribution of Gamma-Ray Bursts to the high-energy diffuse neutrino flux with 10 yr of ANTARES data

A. Albert,^{1,2} M. André,³ M. Anghinolfi,⁴ G. Anton,⁵ M. Ardid,⁶ J.-J. Aubert,⁷ J. Aublin,⁸ B. Baret,⁸ S. Basa,⁹ B. Belhorma,¹⁰ V. Bertin,⁷ S. Biagi,¹¹ M. Bissinger,⁵ J. Boumaaza,¹² M. Bouta,¹³ M. C. Bouwhuis,¹⁴ H. Brânzaş,¹⁵ R. Bruijn,^{14,16} J. Brunner,⁷ J. Busto,⁷ A. Capone,^{17,18} L. Caramete,¹⁵ J. Carr,⁷ S. Celli ^{17,18}★ M. Chabab,¹⁹ T. N. Chau,⁸ R. Cherkaoui El Moursli,¹² T. Chiarusi,²⁰ M. Circella,²¹ A. Coleiro,⁸ M. Colomer-Molla,^{8,22} R. Coniglione,¹¹ P. Coyle,⁷ A. Creusot,⁸ A. F. Díaz,²³ G. de Wasseige,⁸ A. Deschamps,²⁴ C. Distefano,¹¹ I. Di Palma,^{17,18} A. Domi,^{4,25} C. Donzaud,^{8,26} D. Dornic,⁷ D. Drouhin,^{1,2} T. Eberl,⁵ N. El Khayati,¹² A. Enzenhöfer,⁷ A. Ettahiri,¹² P. Fermani,^{17,18} G. Ferrara,¹¹ F. Filippini,^{20,27} L. A. Fusco,^{7,8} P. Gay,^{8,28} H. Glotin,²⁹ R. Gozzini,^{5,22} K. Graf,⁵ C. Guidi,^{4,25} S. Hallmann,⁵ H. van Haren,³⁰ A. J. Heijboer,¹⁴ Y. Hello,²⁴ J. J. Hernández-Rey,²² J. Höfl,⁵ J. Hofestädt,⁵ F. Huang,¹ G. Illuminati,^{8,22} C. W. James,³¹ M. de Jong,^{14,32} P. de Jong,¹⁴ M. Jongen,¹⁴ M. Kadler,³³ O. Kalekin,⁵ U. Katz,⁵ N. R. Khan-Chowdhury,²² A. Kouchner,^{8,34} I. Kreykenbohm,³⁵ V. Kulikovskiy,^{4,36} R. Lahmann,⁵ R. Le Breton,⁸ D. Lefèvre,³⁷ E. Leonora,³⁸ G. Levi,^{20,27} M. Lincetto,⁷ D. Lopez-Coto,³⁹ S. Loucatos,^{8,40} G. Maggi,⁷ J. Manczak,²² M. Marcelin,⁹ A. Margiotta,^{20,27} A. Marinelli,⁴¹ J. A. Martínez-Mora,⁶ S. Mazzou,¹⁹ K. Melis,^{14,16} P. Migliozzi,⁴¹ M. Moser,⁵ A. Moussa,¹³ R. Muller,¹⁴ L. Nauta,¹⁴ S. Navas,³⁹ E. Nezri,⁹ A. Nuñez-Castiñeira,^{7,9} B. O’Ferraigh,¹⁴ M. Organokov,¹ G. E. Pāvālaš,¹⁵ C. Pellegrino,^{20,42,43} M. Perrin-Terrin,⁷ P. Piattelli,¹¹ C. Poirè,⁶ V. Popa,¹⁵ T. Pradier,¹ N. Randazzo,³⁸ S. Reck,⁵ G. Riccobene,¹¹ A. Sánchez-Losa,²¹ D. F. E. Samtleben,^{14,32} M. Sanguineti,^{4,25} P. Sapienza,¹¹ J. Schnabel,⁵ F. Schüssler,⁴⁰ M. Spurio,^{20,27} Th. Stolarczyk,⁴⁰ B. Strandberg,¹⁴ M. Taiuti,^{4,25} Y. Tayalati,¹² T. Thakore,²² S. J. Tingay,³¹ A. Trovato,¹¹ B. Vallage,^{8,40} V. Van Elewyck,^{8,34} F. Versari,^{8,20,27} S. Viola,¹¹ D. Vivolo,^{41,44} J. Wilms,³⁵ A. Zegarelli ^{17,18}★ J. D. Zornoza²² and J. Zúñiga²²

Affiliations are listed at the end of the paper

Accepted 2020 November 6. Received 2020 November 6; in original form 2020 August 5

ABSTRACT

Addressing the origin of the astrophysical neutrino flux observed by IceCube is of paramount importance. Gamma-Ray Bursts (GRBs) are among the few astrophysical sources capable of achieving the required energy to contribute to such neutrino flux through $p\gamma$ interactions. In this work, ANTARES data have been used to search for upward going muon neutrinos in spatial and temporal coincidence with 784 GRBs occurred from 2007 to 2017. For each GRB, the expected neutrino flux has been calculated in the framework of the internal shock model and the impact of the lack of knowledge on the majority of source redshifts and on other intrinsic parameters of the emission mechanism has been quantified. It is found that the model parameters that set the radial distance where shock collisions occur have the largest impact on neutrino flux expectations. In particular, the bulk Lorentz factor of the source ejecta and the minimum variability time-scale are found to contribute significantly to the GRB-neutrino flux uncertainty. For the selected sources, ANTARES data have been analysed by maximizing the discovery probability of the stacking sample through an extended maximum-likelihood strategy. Since no neutrino event passed the quality cuts set by the optimization procedure, 90 per cent confidence level upper limits (with their uncertainty) on the total expected diffuse neutrino flux have been derived, according to the model. The GRB contribution to the observed diffuse astrophysical neutrino flux around 100 TeV is constrained to be less than 10 per cent.

Key words: acceleration of particles – neutrinos – transients: gamma-ray bursts – astroparticle physics.

* E-mail: angela.zegarelli@roma1.infn.it (AZ); silvia.celli@roma1.infn.it (SC)

1 INTRODUCTION

High-energy astrophysical neutrinos were discovered few years ago (Aartsen et al. 2013, 2014, 2015a), opening a new window to the study of the Universe. Identifying the sources of these neutrinos is one of the key scientific targets of the astroparticle physics community. The most powerful accelerators are needed to explain the energetics of these neutrinos and it is possible that their sources generate also Ultra-High-Energy Cosmic Rays (UHECRs), the most energetic particles observed to date, with energies above 10^9 GeV (Zatsepin & Kuzmin 1966; Milgrom & Usov 1995; Waxman 1995; Vietri 1995; Abbasi et al. 2008; Abraham et al. 2010; Globus et al. 2015). Therefore, the discovery of neutrino sources might guide us towards the solution of the one-century-old mystery about the origin of such charged particles.

Among several astrophysical sources, Gamma-Ray Bursts (GRBs) are considered one of the most promising candidate sources of astrophysical neutrinos. They are intense flashes of high-energy electromagnetic radiation, observed isotropically in the sky (Meegan et al. 1992), and thus believed to be of extragalactic nature. GRBs constitute the most powerful known explosions in the Universe, releasing energies between 10^{51} and 10^{54} ergs in a few seconds. For detailed reviews about GRBs, see Piran (2004), Mešzařos (2006), and Zhang & Kumar (2015).

GRBs have historically been observed by space-based facilities, through photons in the energy band from the keV to hundreds of GeV (Ackermann et al. 2014). Recently, the first detections of photons in the sub-TeV energy band from GRB180720B (Abdalla et al. 2019), GRB190114C (Acciari et al. 2019), and from the low-luminous GRB190829A (Valeev et al. 2019; de Naurois 2019) have been carried out with ground-based imaging atmospheric Cherenkov telescopes. Such a novel energetic component has provided further evidence of the powerfulness of this class of accelerators. However, all these sub-TeV observations are thought to be related to the afterglow component of the emission, which is expected when the jet impinges upon the circumstellar medium (Chand et al. 2020; Sahu & López Fortín 2020). On the other hand, the prompt component, which should be produced within the region of particle acceleration, has not been observed yet in TeV gamma rays. The lack of prompt TeV gamma rays seems to be mostly connected to the difficulty faced by ground-based telescopes to follow up the GRB event within the few seconds of duration of the prompt phase. None the less, the discovery of TeV emission has renewed the discussion about the hadronic versus leptonic origin of the observed radiation. Though leptonic scenarios are typically favoured in GRB modelling, the highest energy photons might be witnesses of the onset of a hadronic component (Ghisellini et al. 2020). This fact has clear implications in a multimessenger scenario from the point of view of both follow-up and offline analysis of coincident high-energy neutrinos (see e.g. Dornic et al. 2019).

Multimessenger searches targeted at GRBs appear very promising; being transients and extremely energetic explosions, these sources allow to strongly reduce the background during their very short duration. If hadrons are accelerated in GRBs, neutrinos are expected to be produced by the collisions of protons (or heavier nuclei) on the intense radiation field of the jet. Neutrinos are ideal messengers in the search for distant astrophysical objects, being electrically neutral, stable, and weakly interacting particles. Thus, unlike protons or charged nuclei, neutrinos are not diverted in their path from their source to the Earth. In addition, unlike photons, neutrinos are not absorbed while propagating towards the Earth. For these reasons, searching for a temporal and spatial coincidence among

GRB photons and high-energy neutrinos is crucial to safely identify this kind of sources as hadronic factories and, in addition, to shed light on the composition of their jets.

Over the past years, the two major neutrino telescopes of the Northern and Southern hemispheres, respectively, ANTARES (Ageron et al. 2011) and IceCube (Ahrens et al. 2004), have been searching for neutrino signals coincident with GRBs in time and direction. The lack of detections from these searches has allowed to set progressively stronger upper limits, thus limiting also the possible contribution of these sources to the observed astrophysical diffuse neutrino flux. None the less, current limits do not yet provide significant constraints on the validity of the internal shock model (Piran 1999), once the many uncertainties on parameters that affect the predictions are taken into account.

The results of previous searches of high-energy neutrinos emitted by GRBs with ANTARES data can be found in Adrián-Martínez et al. (2013, 2017a, 2017b), while for IceCube in Aartsen et al. (2015b, 2016, 2017). In the present paper, the search for astrophysical neutrinos from GRBs is extended, including almost 10 yr of ANTARES data. This work differs from previously published results, since it focuses on improving the predictions on the expected neutrino fluences from GRBs. This is achieved by considering the wealth of information accumulated so far thanks to the many astronomical observations, rather than assuming some fixed standard values that do not correctly reproduce the properties of the source sample. Contextually, the different uncertainties due to the poor knowledge of the source dynamics are taken into account and propagated on the produced neutrino spectrum, with the aim of providing a clear understanding of the assumptions and limitations behind the upper limits that are set.

The paper is structured as follows. In Section 2, the ANTARES detector and the data acquisition system are described. In Section 3, the adopted sample for this analysis and the criteria used for selecting the GRB parameters are explained. In Section 4, the neutrino spectra predicted by the internal shock model are discussed, focusing on the uncertainties due to the poor knowledge of some parameters. In Section 5, the analysis chain is described, explaining the Monte Carlo (MC) simulations of GRB neutrino events that provide the detector response to the signal. Then, in Section 6, the estimation of the background that characterizes ANTARES data is presented. In Section 7, the analysis optimization is discussed, through the setup of MC pseudo-experiments generated with the aim of obtaining the highest discovery potential for the neutrino flux by exploiting an extended maximum-likelihood ratio statistical method. In Section 8, the diffuse search performed through the stacking technique, investigating whether the discovery potential can be improved by limiting the analysis to an optimized sub-sample of bursts, is presented. Finally, in Sections 9 and 10, the results of the present analysis are shown.

2 ANTARES DETECTOR AND DATA TAKING

ANTARES (Ageron et al. 2011) is a large volume water–Cherenkov neutrino telescope in the Northern hemisphere, located in the deep water of the Mediterranean Sea, offshore Toulon (France), and fully operational since May 2008. Due to its performances and characteristics, the detector is primarily sensitive to neutrinos in the TeV–PeV energy range. The most relevant neutrino signals for the study of astrophysical sources are the track-like signatures provided by muons, produced by ν_μ charged-current interactions. In this channel, about 50 per cent of the track events are reconstructed within 0.4° of the parent neutrino for an E^{-2} neutrino spectrum (Albert

et al. 2017). The remaining interaction channels produce hadronic and electromagnetic showers that are observed inside the detector as spheres of light radially propagating from the interaction vertex and whose direction is reconstructed with an angular uncertainty of few degrees. For this reason, in this work, the analysis is focused on the track-like signals with better angular resolution.

From the experimental point of view, track-like signals can be either the real tracks induced by muons or the misidentified showers (incorrectly reconstructed as tracks). In order to take into account this possibility, the electron neutrino interactions are also simulated and the track-like events reconstructed from this channel are included in the analysis. In order to reduce the very abundant background coming from atmospheric muons, only upward going events are considered. However, given the very high statistics of atmospheric muons, these have to be further reduced by cuts on the track reconstruction quality. This selection leaves an irreducible background made of atmospheric neutrinos (Gaisser & Hillas 1977).

3 GRB SELECTION AND PARAMETERS

The GRB parameters needed for the search (time, direction) and the simulation of expected neutrino fluxes (photon spectrum, fluence, redshift) are collected from published results of *Swift*¹ (Gehrels et al. 2004), *Fermi*² (Atwood et al. 2009; Meegan et al. 2009), and Konus-Wind³ (Aptekar et al. 1995). Starting with a full sample of GRBs that includes 2604 sources, a selection is performed, satisfying the following criteria:

(i) Short burst are excluded, as this class is poorly understood in terms of neutrino production during their short prompt phase. In other words, only GRBs with prompt duration⁴ $T_{90} \geq 2$ s (the so-called long GRBs) are selected.

(ii) Coordinates of the bursts should be measured by at least one satellite. Those GRBs such that the angular uncertainty provided by the satellite is larger than 10° are excluded.

(iii) The gamma-ray spectrum has to be measured. This is typically fitted with a broken power-law, a cutoff power-law, or a smoothly broken power-law function. It is also required that the spectral indices satisfy the conditions $\gamma_1 > -4$ and $\gamma_2 > -5$, where γ_1 and γ_2 are, respectively, the slope below and above the energy break.

(iv) At least one parameter among electromagnetic fluence and redshift has to be measured, since their values are needed in the calculation of the source luminosity that is primarily affecting the yields in both gamma rays and neutrinos.

(v) Only GRBs that were below the ANTARES horizon at trigger time have been selected.

When physical parameters of a GRB are measured by different detectors, the adopted criteria are:

(i) The burst's position is taken from the detector with the smallest angular error (typically *Swift*–UVOT, then *Swift*–XRT, *Fermi*–LAT, *Swift*–BAT, and finally *Fermi*–GBM).

¹ *Swift* catalogue in https://swift.gsfc.nasa.gov/archive/grb_table/

² *Fermi*–GBM in <https://heasarc.gsfc.nasa.gov/W3Browse/fermi/fermigbrst.html> (Gruber et al. 2014; von Kienlin et al. 2014; Bhat et al. 2016). *Fermi*–LAT in Ajello et al. (2019).

³ Konus-Wind information is available only through the GCN archive: http://gcn.gsfc.nasa.gov/gcn3_archive.html

⁴ T_{90} is the time in which 90 percent of the gamma-ray fluence is emitted, during the so-called prompt phase.

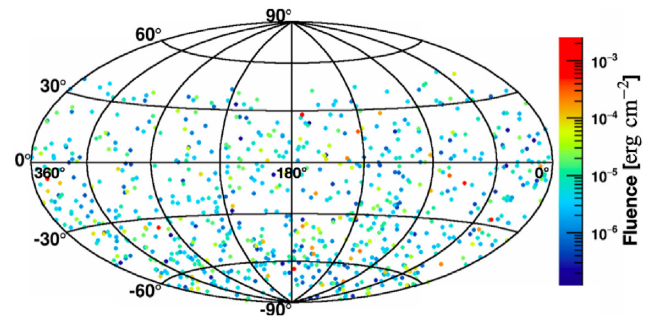


Figure 1. Sky distribution and fluence of the selected 784 GRBs in equatorial coordinates.

Table 1. Percentage contributions of the different satellite catalogues to the determination of GRB position and spectrum. The position of the burst is taken from the detector with the smallest angular error. The spectrum is taken from the satellite with the most extended energy band. The total sample is made up of 784 GRBs.

| Source | Position | Spectrum |
|-------------------------|----------|----------|
| <i>Swift</i> | 29.9% | 16.7% |
| <i>Swift</i> –BAT | 9.3% | |
| <i>Swift</i> –UVOT | 3.4% | |
| <i>Swift</i> –XRT | 17.2% | |
| <i>Fermi</i> | 68.8% | 71.6% |
| Other (e.g. Konus-Wind) | 1.3% | 11.7% |

(ii) The burst's duration, spectrum, and fluence are taken from the satellite reporting measurements in the most extended energy band (typically Konus-Wind 0.02–10 MeV, then *Fermi* 0.01–1 MeV, and finally *Swift* 0.015–0.15 MeV).

Following these criteria, 488 more GRBs have been added with respect to the ones analysed in Adrián-Martínez et al. (2013). The final sample contains 784 GRBs and their spatial distribution in the equatorial sky is shown in Fig. 1. The field of view of the ANTARES detector for upward going events is 2π sr and, due to its geographical location, the sky up to a declination of 47° is visible. The statistics of parameters adopted in this analysis from the several instruments about the source positioning and spectral modelling is specified in Table 1. Note that in some cases, some parameters have not been measured, e.g. in many cases, the information on the energy break is missing, as well as the spectral slope above it. In such a situation, default values are assumed: the peak energy of the burst is set at 200 keV when unknown (33 percent of the cases) and $\gamma_2 = \gamma_1 - 1$ when only γ_1 is available from catalogues (1.4 percent of the cases). Moreover, the host galaxy of the GRB can fail to be identified by the multiwavelength follow-up and so the redshift remains unknown. With respect to the redshift, former analyses have been adopting the default value $z = 2.15$ in case this information was not available. In addition, for the minimum variability time-scale t_v of the bursts, which can be determined by the width of the peaks in the light curve, a default value of $t_v = 10$ ms (derived from theoretical consideration put forward in Guetta et al. 2004) has been used so far in all neutrino searches. However, since these parameters affect crucially the GRB–neutrino fluence estimation, a different strategy has been adopted here, as explained in Section 4.2.

4 COMPUTATION OF THE NEUTRINO FLUX FROM INTERNAL SHOCKS

The most commonly accepted scenario to explain the physics of GRBs is the so-called fireball model (Rees & Mešzařos 1992), where the stellar explosion drives the relativistic expansion of a plasma of particles. According to the internal shock framework of the fireball model (Kobayashi, Piran & Sari 1997; Daigne & Mochkovitch 1998; Piran 1999), the central engine of GRBs produces multiple shells with different speeds: the faster ones catch up with the slower ones and collide. The acceleration mechanism converts part of the jet's kinetic energy into internal energy (Piran 2004) and a fraction of this energy is expected to be transferred to non-thermal particles, achieving relativistic speeds. Accelerated electrons subsequently lose their energy through synchrotron and inverse Compton processes. The intense emitted radiation field constitutes the target for photo-hadronic interactions with the protons accelerated at shock fronts: from these collisions, mesons are produced, which then decay, generating neutrinos and gamma rays. These processes constitute the so-called prompt phase of the emission. None the less, if GRBs were purely leptonic sources (Asano & Terasawa 2009), the observed radiation would be completely ascribed to processes involving primary electrons, such that there would be no possibility to produce neutrinos in these sources.

In a simplified one-zone emission model, a single representative collision is realized at the so-called internal shock radius, located at a distance

$$R_{\text{is}} \simeq \frac{2\Gamma^2 c t_v}{(1+z)} \simeq 2 \times 10^{13} \left(\frac{t_v}{0.01 \text{ s}} \right) \left(\frac{\Gamma}{10^{2.5}} \right)^2 \left(\frac{3}{1+z} \right) \text{ cm} \quad (1)$$

from the central emitter. Note that the internal shock radius strongly affects the characteristic energy range of emitted neutrinos, while simultaneously scaling the normalization of the neutrino spectrum (Guetta et al. 2004). As equation (1) shows, the Lorentz factor impacts significantly the spectral modelling. In addition, the variability time t_v is expected to be a crucial parameter as well, given its broad range of variation among GRBs. It is also worth mentioning that some models (Lyutikov 2006; Kumar & McMahon 2008) have argued emission radii larger than what indicated by equation (1), correspondingly predicting a less efficient neutrino production. Interestingly, these models favour the interpretation of GRBs as sources of UHECRs (Murase et al. 2008; He et al. 2012), as heavy nuclei would be allowed to survive without being disintegrated.

Furthermore, neutrino production is thought to be efficiently realized also at radii below the photosphere, namely the location where the optical depth of Thomson scattering along the jet falls to unity, which is expected to be located at $R_{\text{ph}} \sim 10^{12}$ cm. In the photospheric scenario (Paczynski 1986; Thompson 1994; Mešzařos & Rees 2000; Murase 2008; Murase, Kashiyama & Mešzařos 2013; Zhang & Kumar 2013), because the dissipation radius is located closer to the central engine ($R_{\text{ph}} < R_{\text{is}}$), the characteristic energy range where photospheric neutrinos are expected to be detected is typically lower than what is expected in the internal shock model. It follows that, in order to test the photospheric model, special data acquisition conditions are required so as to access events with a low-level trigger. The interested reader is referred to Adrián-Martínez et al. (2017b) for a dedicated study on the photospheric model as applied to some interesting bright GRB events. In turn, the present work will be focused on testing the internal shock scenario.

The neutrino flux expected from GRBs during the prompt phase was first computed analytically by Paczynski & Xu (1994) and Waxman & Bahcall (1997), while refined calculations were per-

formed in the following years (Guetta et al. 2004; Murase & Nagataki 2006; Murase et al. 2008; Hümmer et al. 2010; Hümmer, Philipp & Winter 2012). Among such approaches, the numerical method developed by Hümmer et al. (2010) and, later on, by Hümmer et al. (2012) is adopted in the present work.

4.1 The numerical modelling with NeuCosmA

The event generator ‘Neutrinos from Cosmic Accelerator’ (NeuCosmA) (Hümmer et al. 2010, 2012), used in this work to compute the expected neutrino fluxes, is based on the assumption that protons are accelerated through first-order *Fermi* processes (Bell 1978) (i.e. with a differential energy spectrum $\propto E^{-2}$) in the relativistic ejecta of the burst and interact with the intense jet photon field. The latter is described by an energy distribution in the form of a broken power-law function (Band et al. 1993) constrained by observations.

The adopted version of NeuCosmA assumes a one-zone collision, namely it simulates average shell properties, such as an average shock speed or Lorentz factor Γ (i.e. the bulk Lorentz factor of the jet). Indeed, it can be considered as an approximation that the ejecta coast with constant bulk Γ before decelerating due to the interaction with the external medium (Zhang & Kumar 2015). Note that in a more realistic situation, the collisions between plasma shells are different one from the other, each happening under different physical conditions, as the irregular burst light curves demonstrate. The latest release of the NeuCosmA code allows to account for such a multicollisions scenario (Bustamante et al. 2015, 2017) by modelling the specific light curve of individual GRBs. However, given the extended sample of sources considered in this work, the one-zone collision approach, which rather relies on the average spectral properties of the bursts, is adopted.

Since the synchrotron-emitted photons constitute the radiation field on which accelerated protons collide, the normalization of the neutrino fluence depends linearly on the intensity of the photon flux and on the ratio of fireball energy in protons to electrons. This so-called baryonic loading, f_p , is an unknown of the problem, possibly constrained by neutrino observations. From the theoretical point of view, a reasonable value for it could be $f_p \simeq 10$ (Hümmer et al. 2012); such a value will be fixed in the following for each GRB considered. The normalization of the neutrino fluence depends on other several quantities (Hümmer et al. 2012):

- (i) The total fraction of the energy transferred from protons to pions. Considering the reaction kinematics, approximately 20 per cent of the proton energy are transferred to the produced pion in each interaction.
- (ii) The isotropic gamma-ray luminosity of the burst, $L_{\gamma, \text{iso}}$. It is given by $L_{\gamma, \text{iso}} = 4\pi d_L^2 F_{\gamma} / T_{90}$, where F_{γ} is the bolometric gamma-ray fluence (1 keV–10 MeV), T_{90} is used as a proxy for duration, and d_L is the luminosity distance of the source.
- (iii) The minimum variability time-scale t_v that is directly connected to the size of the emitting radius R_{is} through equation (1) (Guetta et al. 2004).
- (iv) The peak value of the gamma-ray energy spectrum E_{peak} .

4.2 Uncertainties in neutrino flux computation

Unfortunately, the intrinsic parameters of the emission regions, like the boost Lorentz factor Γ and the variability time-scale t_v , cannot reliably be determined on a source-by-source basis. In few cases, the Lorentz factor can be estimated: in the so-called ‘afterglow onset method’ (Sari & Piran 1999), one can relate the energy break

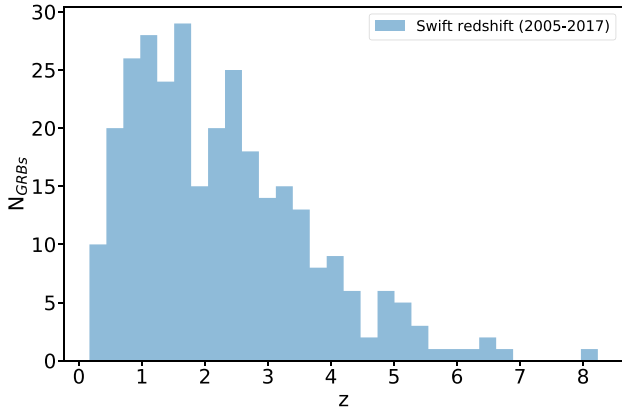


Figure 2. *Swift* redshift distribution for GRBs detected from 2005 to 2017 (data are available in : <https://swift.gsfc.nasa.gov/archive/grb-table/>).

observed in the GRB light curve during the afterglow phase to the jet deceleration time and hence to the initial jet speed. Alternatively, one can use the maximum energy of observed photons (Lithwick & Sari 2001; Gupta & Zhang 2008; Abdo et al. 2009b, a, c) or the quiescent periods between the prompt emission pulses, in which the signal of external shock is expected below the instrument threshold (Zou & Piran 2010) to infer an average Γ of the jet. The former approach was, for instance, adopted in Lü, Zou & Lei (2012) for a sample of 38 GRBs from which the authors could derive the following correlation between the Lorentz factor Γ and the mean isotropic gamma-ray luminosity $L_{\gamma, \text{iso}}$:

$$\Gamma \simeq 249(L_{\gamma, \text{iso}, 52})^{0.30}, \quad (2)$$

where $L_{\gamma, \text{iso}, 52} \equiv L_{\gamma, \text{iso}}/(10^{52} \text{ erg s}^{-1})$. Therefore, by knowing the isotropic luminosity of the burst, it is possible to infer the jet Lorentz factor. However, the application of this method is not free from uncertainties, as the isotropic luminosity is also often unknown. In fact, in order to derive $L_{\gamma, \text{iso}}$, the knowledge of the redshift is required (because of the luminosity distance $d_L = d_L(z)$). As redshift is known only in 11 per cent of the cases, a method accounting for the observed redshift distribution of long GRBs was applied in order to estimate, respectively, (i) luminosity distance, (ii) isotropic gamma-ray luminosity, and (iii) bulk Lorentz factor for each GRB in the selected sample. Specifically, 1000 random extractions of the z value are performed for GRBs with unknown z , according to the redshift distribution of long GRBs, as observed by *Swift* since 2005 and shown in Fig. 2. It is worth mentioning that the introduction of such a distribution in this analysis does not introduce any bias, as it can be shown that the *Swift* z -distribution is representative of the entire sample of long GRBs detected by any instrument from 1997 until today. Nevertheless, the *Swift* distribution appears very suitable for the purpose of the present analysis, as it can be easily accessed through the satellite’s online catalogue. Therefore, for each GRB whose redshift measurement is missing, a value of z is assigned, which allows to first compute the luminosity distance d_L and then $L_{\gamma, \text{iso}}$. Note that the resulting value of isotropic luminosity is also required to be between 10^{49} and $10^{54} \text{ erg s}^{-1}$ since this is the luminosity interval where long GRBs are detected. Further details on this method and the resulting Γ distribution obtained for the selected GRB sample are provided in Appendix A.

A similar procedure of random extraction according to a known distribution of values is adopted for the minimum variability time-scale t_v , which is known only in the 33 per cent of the cases. For

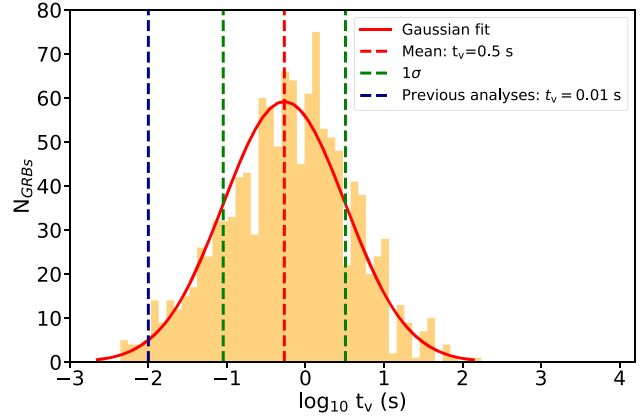


Figure 3. Distribution of minimum variability time-scales obtained analysing 1213 GRB light curves (Golkhou & Butler 2014; Golkhou et al. 2015; Sonbas et al. 2015). The solid red line indicates the Gaussian fit of the distribution. The dashed red line is the mean of the distribution from which a mean value of $t_v = 0.5 \text{ s}$ is obtained. The dashed green lines indicate the 1σ level. The dashed blue line indicates the default value $t_v = 10 \text{ ms}$, previously adopted e.g. in Adrián-Martínez et al. (2013) and Aartsen et al. (2017).

this reason, a distribution of known values of t_v for long GRBs, as obtained from Fourier analyses on burst light curves (Golkhou & Butler 2014; Golkhou, Butler & Littlejohns 2015; Sonbas et al. 2015), is built as shown in Fig. 3. For each GRB with unknown t_v , 1000 values of such parameter are randomly extracted from this distribution. Note that the default value previously adopted in ANTARES GRB search (Adrián-Martínez et al. 2013) and advocated in Guetta et al. (2004), $t_v = 10 \text{ ms}$, is actually located in the tail of the measured distribution, which on the other hand peaks around 0.5 s . Clearly, the default values assumed so far are not representative of the different properties of the GRB population.

Hence, by using the extracted values of redshift z and variability time-scale t_v , 1000 fluxes for each GRB (for which z and/or t_v are unknown) are simulated, in order to estimate the final neutrino fluence by assuming values of the unknown parameters spanning their allowed ranges. The method allows also to investigate how these uncertainties affect the neutrino spectra and to identify the parameter that contributes the most. Therefore, the following procedure is adopted for those sources lacking both z and t_v :

- (i) Calculate the average neutrino fluence resulting from the 1000 simulations.
- (ii) Use the standard deviation σ of the obtained distribution as uncertainty on the average fluence.
- (iii) Provide the results in terms of $E_{\nu\mu}^2 F_{\nu\mu} \pm 2\sigma$.

When both z and t_v are known (30 GRBs in the sample), the statistical error around the flux is obtained by propagating the measured parameter uncertainties on $E_{\nu\mu}^2 F_{\nu\mu}$. In such cases, the uncertainties are so small that the relative difference between $E_{\nu\mu}^2 F_{\nu\mu}$ and $E_{\nu\mu}^2 F_{\nu\mu} \pm 2\sigma$ is negligible, of the order of 10^{-1} in the worst cases. However, in few cases, the uncertainty on redshift is not available from measurements: in these cases, the uncertainty has been considered on the last significant digit. In Appendix B, few examples referring to the different cases here explained are reported.

With respect to the correlation adopted in equation (2), it is worth noting that several expressions of it exist in the literature, which mainly differ in the observational strategy and physical description of the GRB evolution they rely upon. For instance,

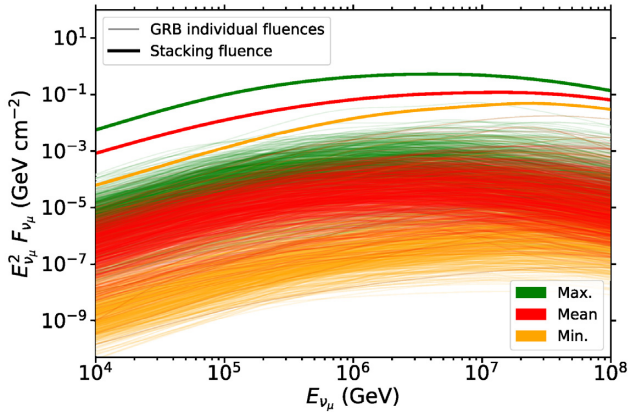


Figure 4. Individual fluences calculated for each GRB of the 784 in the sample (thin lines) and the corresponding stacked fluence (thick line), calculated as in equation (3). The mean ($E_{\nu_\mu}^2 F_{\nu_\mu}$), minimum ($E_{\nu_\mu}^2 F_{\nu_\mu} - 2\sigma$), and maximum ($E_{\nu_\mu}^2 F_{\nu_\mu} + 2\sigma$) fluences are shown in red, orange, and green, respectively.

Ghirlanda et al. (2012) found a relation between Γ and the peak luminosity $L_{\gamma, \text{peak}}$ by relying on the backwards extrapolation of the self-similar deceleration solution for the shock evolution, as derived by Blandford & McKee (1976) (BM). With respect to the method here adopted, the Ghirlanda et al. (2012) approach comes with two further assumptions: (i) that in correspondence of the deceleration stage, the system dynamics has entered the BM self-similar solution and (ii) that the intersection of the two asymptotic power-law phases adopted to describe the shock evolution corresponds to the observed peak time of the afterglow light curve. Because of these stringent limitations, this analysis will adopt the standard approach for the Γ estimation by Lü et al. (2012). Clearly, this choice impacts the neutrino flux expectations, in that a significantly different evaluation of the bulk Lorentz factor might lead to a variation in the expected location of the internal shock radius [see equation (1)]. As the neutrino flux is expected to be extremely sensitive to the Lorentz factor (He et al. 2012), a treatment of the additional systematics associated with adopting a different method for deriving Γ is presented in Appendix C.

4.3 Cumulative neutrino fluence from all GRBs in the sample

By summing over all the individual neutrino fluences, the total fluence expected from the cumulative contribution of the selected 784 GRBs in the period 2007–2017 is calculated as:

$$E_{\nu_\mu}^2 F_{\nu_\mu} = \sum_{i=1}^{N_{\text{GRB}}=784} (E_{\nu_\mu}^2 F_{\nu_\mu})^i. \quad (3)$$

In Fig. 4, the expected minimum, mean, and maximum fluences, respectively, defined as $E_{\nu_\mu}^2 F_{\nu_\mu} - 2\sigma$, $E_{\nu_\mu}^2 F_{\nu_\mu}$, and $E_{\nu_\mu}^2 F_{\nu_\mu} + 2\sigma$ are shown for each GRB and for the whole sample. Focusing on the total fluence, note that the maximum and minimum fluences define the error band around the mean one, shown in Fig. 5. It is possible also to convert the total neutrino fluence of the sample of N_{GRB} into the quasi-diffuse neutrino flux induced by the same sources by rescaling the total fluence with the average rate of GRBs distributed over the full sky expected per year. Hence, the quasi-diffuse neutrino flux is

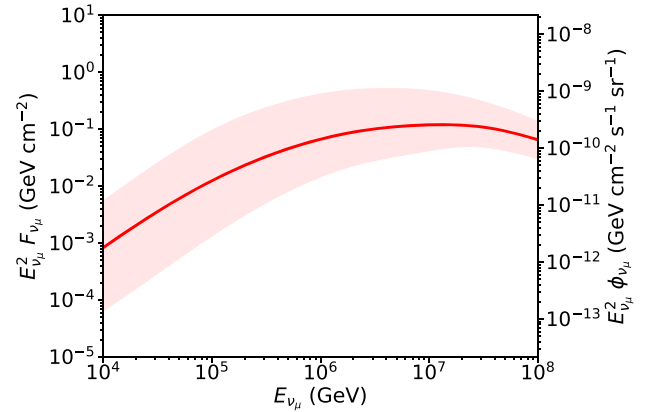


Figure 5. Total neutrino fluence $E_{\nu_\mu}^2 F_{\nu_\mu}$, expected from the 784 GRBs in the sample selected in the period 2007–2017 (left-hand axis), as in equation (3), and corresponding quasi-diffuse neutrino flux $E_{\nu_\mu}^2 \phi_{\nu_\mu}$ (right-hand axis), as defined in equation (4). The shaded region indicates the error band, obtained from the sum of the individual maximum and minimum fluences for each GRB in the sample (see Fig. 4).

obtained as

$$E_{\nu_\mu}^2 \phi_{\nu_\mu} = \sum_{i=1}^{N_{\text{GRB}}} (E_{\nu_\mu}^2 F_{\nu_\mu})^i \frac{1}{4\pi} \frac{1}{N_{\text{GRB}}} 667 \text{yr}^{-1}, \quad (4)$$

where an annual rate of long GRBs equal to 667 per year is considered, in agreement with the previous ANTARES analyses (Adrián-Martínez et al. 2013, 2017a). The diffuse neutrino flux computed with this method is indicated in the right-hand axis of Fig. 5. This quantity is actually more interesting than the total expected fluence, since it allows to compare the neutrino flux produced by the GRBs in the analysis with both the sensitivity of neutrino telescopes and the measurement of the astrophysical neutrino flux reported by IceCube, in order to constrain the contribution of GRBs to this flux (refer to Section 9 for more details).

5 SIGNAL SIMULATION: THE DETECTOR PROBABILITY DENSITY FUNCTION

For each source in the sample, an MC simulation of the expected signal is performed in the so-called run-by-run mode, i.e. accounting for the specific detector condition at the time that the GRB occurred, in the same way as in Adrián-Martínez et al. (2013). In this way, the event generation is able to accurately describe the data taking and calibration conditions of the detector during the run in which each GRB happened. Both tracks, resulting from ν_μ charged current interactions (CC), and showers, produced at ν_μ neutral current (NC) as well as at ν_e both CC and NC interactions, are included in the simulation and signal events are generated from the specific location of the sky where the GRB was observed by gamma-ray satellites. To take the ANTARES absolute pointing uncertainty into account, the GRB local coordinates used in the MC signal production are shifted of a quantity randomly generated following Adrián-Martínez et al. (2012a) and Albert et al. (2017) (see also Albert et al. 2018, 2020 for other studies on the ANTARES pointing accuracy).

Since only GRBs below the ANTARES horizon at the trigger time are considered in this search to reduce the atmospheric muon background, neutrinos are simulated from the direction of the GRB and passing through the Earth, following the simulation scheme described in Adrián-Martínez et al. (2012b). Upward-going muon tracks are

then reconstructed, to compute the acceptance of the detector, with the same algorithm as in Adrián-Martínez et al. (2013). The quality of the reconstruction is estimated through two parameters: Λ , the track-fit quality parameter, and β , the estimated angular uncertainty on the muon track direction (Aguilar et al. 2011). To improve the signal-to-noise ratio, to ensure a good-quality reconstruction, and also to limit the atmospheric muon contamination, only tracks with $\beta < 1^\circ$ are considered in the analysis. The search is then optimized through varying a cut on Λ selecting tracks above a given threshold Λ_{cut} , as explained in Section 8.

The distribution of the angular distance between the reconstructed track direction (for each Λ_{cut}) and the GRB's coordinates, normalized to the total number of events, defines the signal Probability Density Function (PDF) $S(\alpha) = dN(\alpha)/d\Omega$, where α is the angular distance between the simulated GRB position and the reconstructed muon direction and $d\Omega$ is the differential solid angle $d\Omega = 2\pi \sin\alpha d\alpha$. The signal PDF is fitted with a function that is flat for small values of α and by a Rayleigh distribution (Rayleigh 1880) for larger values.

6 BACKGROUND ESTIMATION

The expected number of background events μ_b associated to each GRB, at zenith θ and azimuth ϕ , is evaluated directly from data collected by ANTARES off source and off time (between 2007 December 27 and 2017 December 30) as:

$$\mu_b(\theta, \phi)_{\text{GRB}} = 1.5 T_s \cdot \langle n(\theta_{\text{GRB}}, \phi_{\text{GRB}}) \rangle \cdot C, \quad (5)$$

where T_s is the temporal time window around the GRB occurrence, C is the detector efficiency in the specific runs where each GRB occurred, and $\langle n(\theta_{\text{GRB}}, \phi_{\text{GRB}}) \rangle$ is the time-averaged rate of events reconstructed in the GRB direction. In the framework of prompt GRB emission, the temporal search window of the neutrino signal was defined in coincidence with the gamma-ray signal, slightly extended to account for uncertainties due to the gamma-ray duration of the event, to the ANTARES data acquisition system, and to the propagation time of particles from the satellite to our detector. The time-averaged rate of events reconstructed in the GRB direction is here estimated with a sample of 15657 runs, equivalent to 61562.5 h of livetime (~ 2565 d). To be conservative, this average value is compared with the mean of time-averaged rates within a 10° cone around the GRB position, choosing the highest between these two values. This is performed in fact as to account also for the non-uniformity of the background in the vicinity of the GRB position. Finally, in equation (5), the factor 1.5 is included to conservatively increase the background estimate by 50 per cent.

The background PDF, $B(\alpha) = dN(\alpha)/d\Omega$ is assumed to be flat in Ω within the search cone angle, assuming the value as calculated in equation (5). As a result, the average number of background events expected within a search cone of 10° around a given GRB position is found to be of the order of 10^{-4} .

For a more detailed description of the signal simulation and background estimation described, see Adrián-Martínez et al. (2013).

In Fig. 6, the results of the entire analysis chain for a particular GRB (taken as an example), GRB111123A, are presented. The figure shows the signal and background PDFs up to a distance of 10° from the simulated GRB position. The signal PDF is obtained by considering all the neutrino events simulated that have been reconstructed as tracks with $\Lambda_{\text{cut}} = -5.2$. The median

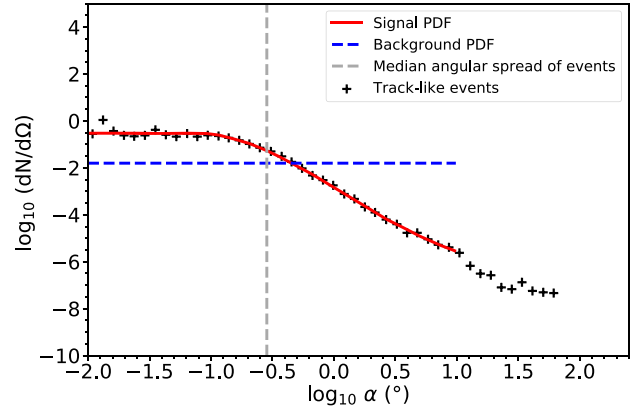


Figure 6. GRB111123A: reconstructed events from the MC signal simulation, per solid angle Ω as a function of the logarithm of the space angle α , obtained with tracks from ν_μ CC interactions and tracks from ν_μ NC and ν_e NC + CC interactions (all neutrino channels are shown in black), with $\beta < 1^\circ$ and $\Lambda_{\text{cut}} = -5.2$. The vertical dashed line (in grey) indicates the median angular spread of events ($\langle \alpha \rangle = 0.29^\circ$); the horizontal dashed line (in blue) shows the flat background PDF $B(\alpha)$. The red curve is the signal Point Spread Function (PSF), inside the defined angular window, 10° , around the GRB position.

angular spread of events (i.e. the median angular resolution) is also provided.

7 MAXIMUM LIKELIHOOD AND PSEUDO-EXPERIMENTS

MC pseudo-experiments are simulated individually for each GRB with the aim of constructing an ensemble of independent replications of the data acquisition and computing the significance of the measurement.

For each GRB, different sets of simulations are generated by varying Λ_{cut} from -5 to -5.8 . For each of these cuts, $\sim 4 \times 10^6$ signal events and $\sim 4 \times 10^{11}$ background events are simulated. A test statistics Q , defined as the ratio between the likelihood in the hypothesis of signal plus background and the likelihood in the background only hypothesis, is evaluated in the form of an ‘extended maximum likelihood ratio’ (Barlow 1990). Furthermore, to determine the statistical significance of measurements, the p value⁵ is calculated, i.e. the probability to yield Q values at least as high as that observed if the background-only hypothesis was true. At the end of this procedure, the optimal cut on the quality parameter, Λ_{cut} , is chosen as the one maximizing the Model Discovery Potential (MDP), i.e. the probability to observe an excess with a p value lower than the pre-defined threshold at a given statistical accuracy assuming the signal predicted by the theoretical model (NeuCosmA).

This strategy was already used by Adrián-Martínez et al. (2013) and by Adrián-Martínez et al. (2017b). However, there is a difference here in the MDP calculation: the systematic uncertainties in the ANTARES acceptance, which translate into a systematic uncertainty on the value of the estimated signal μ_s , are considered in this work, consistently with other previous ANTARES analyses on neutrino sources (Adrián-Martínez et al. 2012b; Albert et al. 2017).

⁵The two-sided convention is used here, namely $p_{3\sigma} = 2.7 \times 10^{-3}$, $p_{4\sigma} = 6.3 \times 10^{-5}$, and $p_{5\sigma} = 5.7 \times 10^{-7}$.

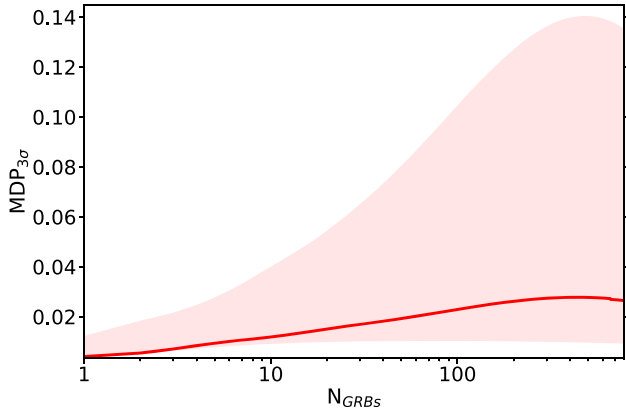


Figure 7. Model Discovery Potential at 3σ , $MDP_{3\sigma}$, as a function of the number of stacked GRBs, N_{GRBs} . The thick red line indicates the $MDP_{3\sigma}$ obtained with the mean neutrino fluence, while the shaded region is the uncertainty on $MDP_{3\sigma}$ obtained by considering the minimum and maximum fluences (see Fig. 4).

8 STACKING ANALYSIS AND SEARCH OPTIMIZATION

The procedure of stacking sources consists into the definition of a GRB sub-sample that includes in the analysis, among the GRBs sample defined in Section 3, as many candidates in terms of neutrino emission as necessary to obtain the best sensitivity. The progressive inclusion of promising GRBs implies the addition not only of the signal but also of the background that they enclose. For this reason, the optimal number of sources to stack is found as a compromise between the statistical reduction and the signal gain due to an increasing number of sources in the final sample. In particular, it corresponds to the value that maximizes the probability to make a significant discovery (MDP). The procedure, described in details in Adrián-Martínez et al. (2013), has been optimized for a 3σ significance level. In Fig. 7, it is possible to see that the loss in $MDP_{3\sigma}$ is very limited between the use of the whole sample and of an optimal one. Hence, the stacking is performed on the whole GRB sample (784 GRBs). Though the search is not optimal in terms of cumulative $MDP_{3\sigma}$, the track quality cut Λ_{cut} is set to optimize the $MDP_{3\sigma}$ of individual GRBs. In this regard, the most promising 10 GRBs at 3σ are reported in Table 2, together with the search time window, the optimized cuts, and the corresponding expected number of background and signal events.

The results of the stacking of all 784 sources are presented in Section 9, corresponding to an $MDP_{3\sigma} = 0.027$ (0.009; 0.136), where the values within parentheses represent the range of $MDP_{3\sigma}$ values when the model parameters are allowed to vary within 3σ .

9 RESULTS AND DISCUSSION

ANTARES data from the end of 2007–2017 are analysed according to the cuts identified in the optimization procedure presented above, searching for neutrino events in spatial and temporal coincidence with the prompt phase of GRBs observed by satellite-based gamma-ray instruments. No neutrino events have passed the selection criteria defined through the optimization procedure and, thus, no neutrino events are found in spatial and temporal coincidence with the GRB sample for an equivalent livetime of the search of 18.9 h. The corresponding 90 per cent confidence level (CL) upper limit on the

Table 2. Optimization results obtained with mean fluences: the first 10 GRBs with the highest $MDP_{3\sigma}$ are shown, with the corresponding optimized Λ_{cut} value, the expected number of background μ_b , and signal μ_s events at 3σ and the T_s . In the last rows, the sum and mean of the values for all 784 GRBs at 3σ are given. The naming convention of the GRBs is as the same as used by *Fermi* (see <https://heasarc.gsfc.nasa.gov/W3Browse/fermi/fermigbrst.html>).

| GRB | Λ_{cut} | μ_b (events) | μ_s (events) | T_s (s) | $MDP_{3\sigma}$ |
|-----------|-----------------|----------------------|----------------------|-------------------|----------------------|
| 13042732 | −5.5 | 5.3×10^{-5} | 2.2×10^{-3} | 33.9 | 2.1×10^{-3} |
| 10072809 | −5.5 | 9.7×10^{-5} | 1.1×10^{-3} | 268.6 | 9.8×10^{-4} |
| 17101079 | −5.3 | 1.0×10^{-4} | 1.0×10^{-3} | 252.0 | 9.4×10^{-4} |
| 09072071 | −5.4 | 1.8×10^{-5} | 7.8×10^{-4} | 21.2 | 6.7×10^{-4} |
| 11092889 | −5.4 | 4.4×10^{-4} | 5.1×10^{-4} | 115.0 | 4.3×10^{-4} |
| 14041606 | −5.4 | 5.5×10^{-5} | 4.2×10^{-4} | 36.8 | 4.0×10^{-4} |
| 12070780 | −5.5 | 7.9×10^{-5} | 4.1×10^{-4} | 69.5 | 3.8×10^{-4} |
| 11122865 | −5.5 | 4.0×10^{-4} | 4.4×10^{-4} | 163.7 | 3.6×10^{-4} |
| 14081078 | −5.4 | 7.6×10^{-5} | 3.7×10^{-4} | 97.7 | 3.6×10^{-4} |
| 10091081 | −5.3 | 5.4×10^{-5} | 3.4×10^{-4} | 27.3 | 3.2×10^{-4} |
| All GRBs: | | | | | |
| Mean | −5.3 | 9.4×10^{-5} | 3.8×10^{-5} | 86.9 | 3.4×10^{-5} |
| Sum | | 7.3×10^{-2} | 3.0×10^{-2} | 6.8×10^4 | 2.7×10^{-2} |

computed neutrino signal ϕ_{ν_μ} is calculated as

$$\phi_{\nu_\mu}^{90\%} = \phi_{\nu_\mu} \frac{\mu_s^{90\%}}{n_s} = \phi_{\nu_\mu} \frac{2.3}{n_s} = \phi_{\nu_\mu} \cdot 77_{-64}^{+226}, \quad (6)$$

where the expected number of signal events from the total sample, n_s , is estimated to be

$$n_s(N_{GRB} = 784) = 0.03_{-0.02}^{+0.14}. \quad (7)$$

The factor 2.3 is the 90 per cent CL upper limit of the mean of a Poisson process and the value in equation (7) is a result of the optimization procedure applied on minimum, mean, and maximum fluences, as explained in Section 8. Note that the relative uncertainty on the expected number of signal events is smaller than the one estimated on the MDP; in other words, the neutrino flux uncertainty due to unknown model parameters is quite limited in the energy range that is relevant for our search. Still, the uncertainty here presented is only partial, as it does not account for the systematics associated with having fixed the correlation in equation (2) to derive the bulk Lorentz factor, which is the parameter expected to most affect the neutrino flux (He et al. 2012). In Appendix C, such a contribution is also evaluated: as a result of adopting the correlation from Ghirlanda et al. (2012), the expected neutrino flux is observed shifted to lower energies and with a larger normalization, leading to a significantly larger number of expected neutrino events. However, the experimental cuts obtained with an independent optimization procedure are found to remain almost unaltered. As a consequence, the absence of neutrinos associated to GRBs in ANTARES data allows constraints on both models to be derived. The 90 per cent CL upper limits so obtained lay at a comparable level. For the cumulative fluence of equation (3), this limit reads as $1.3_{-0.8}^{+4.1} \times 10^{-2} < E_{\nu_\mu}^2 F_{\nu_\mu} < 0.8_{-0.7}^{+5.2} \times 10^{-1} \text{ GeV cm}^{-2}$, in the energy range extending from $6.3 \times 10^4 \text{ GeV}$ to $1.3 \times 10^7 \text{ GeV}$, which is the region where 90 per cent of the mean fluence is expected to be detected by ANTARES. The fluence limit translates into $1.3_{-0.8}^{+4.1} \times 10^{-9} < E_{\nu_\mu}^2 \phi_{\nu_\mu} < 1.0_{-0.5}^{+0.9} \times 10^{-8} \text{ GeV cm}^{-2} \text{ s}^{-1} \text{ sr}^{-1}$ in terms of quasi-diffuse flux (cf. equation 4). The quasi-diffuse expected flux and corresponding upper limit, as calculated from the mean expected fluence, are shown in Fig. 8 and compared to previous ANTARES limits (Adrián-Martínez et al. 2013). An improvement by a factor of ~ 2 on the 90 per cent CL upper limit can be observed, due to the increased sample statistics, jointly with having here adopted

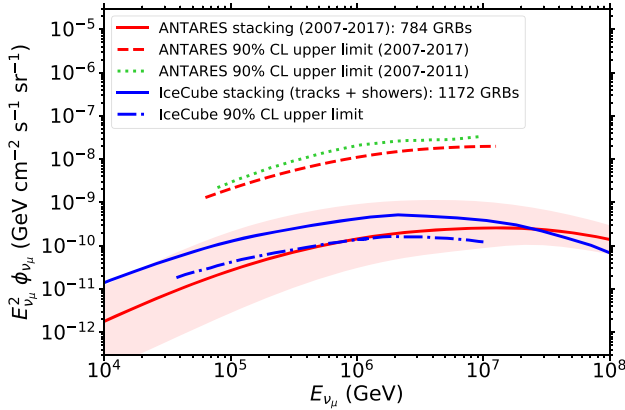


Figure 8. Comparison between the 90 per cent CL upper limit (red dashed line) with respect to the ANTARES expected quasi-diffuse flux for 784 GRBs (red solid line), in equation (4), and the previous ANTARES 90 per cent CL upper limit (green dashed line) (Adrián-Martínez et al. 2013). The solid blue line represents the quasi-diffuse flux expected by IceCube for 1172 GRBs and the corresponding dash-dotted blue line shows the corresponding 90 per cent CL upper limit (Aartsen et al. 2017).

a more realistic model for neutrino predictions including a detailed study on the model parameters. The results are also compared with the latest IceCube all-sky search (Aartsen et al. 2017), where no statistically significant signal was found by combining both track and shower events for 1172 GRBs. From this comparison, it is possible to appreciate that the GRB-neutrino flux expected by IceCube is consistent with the one presented in this work over the entire energy range of 10^4 – 10^8 GeV, the former being on average higher than the latter due to the larger sample size. The same spectral trend is reflected in individual upper limits. It is worth keeping in mind that when comparing results from different analyses, one should consider that the spectral and limit shapes depend on the selected sample, the measured parameters of each burst, and their uncertainty, namely the set of parameters that are introduced in the chosen model. Here, for the first time, no default value for the model parameters is used and more physical and realistic values are considered (see Section 4.2).

Finally, the expected quasi-diffuse neutrino flux from the selected 784 GRBs and the corresponding upper limit can be compared with the diffuse astrophysical flux observed by IceCube. To this extent, Fig. 9 provides the IceCube best fits of the neutrino flux, in both the 10 yr ν_μ track data sample (Stettner et al. 2019) and the 7.5-yr High-Energy Starting Events (HESE)⁶ sample (Schneider et al. 2019). To allow a more significant comparison, the upper limit derived from this search is reported with its error band [see equation (6)]. By comparing the ANTARES upper limit with the diffuse astrophysical neutrino flux observed by IceCube, it is possible to conclude that GRBs are not the main contributors to the observed flux below $E_\nu \sim 1$ PeV, within the NeucosMA model framework set with benchmark baryonic loading ($f_p = 10$). This result confirms previous searches performed by IceCube (Aartsen et al. 2015b, 2016, 2017). In particular, in the energy region where ANTARES is most sensitive, i.e. below ~ 100 TeV, GRBs do not contribute by more than 10 per cent. Consequently, the parameter space still allowed to the

⁶The neutrino interaction vertex is located inside the detector and its energy is larger than 20 TeV.

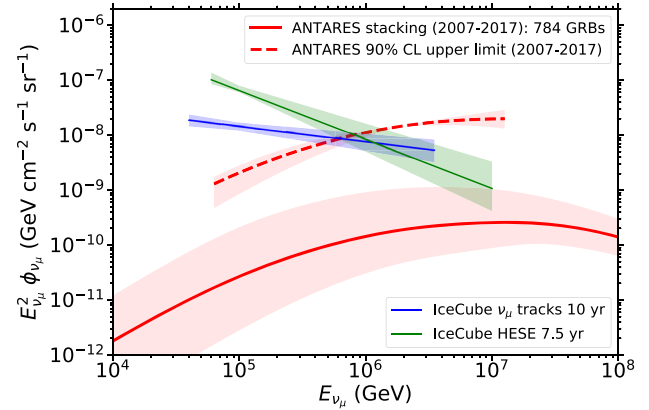


Figure 9. GRB ANTARES quasi-diffuse flux for 784 GRBs, in equation (4), (red solid line) and the corresponding 90 per cent CL upper limit (dashed red line). The red shaded regions show the uncertainty around the GRB quasi-diffuse flux, as in Fig. 5, and also around the computed upper limit, derived as explained in Section 8. IceCube best fits for ν_μ tracks in 10 yr (Stettner et al. 2019) and for HESE events in 7.5 yr of collected data (Schneider et al. 2019) are shown in blue and green, respectively.

internal shock model is characterized by sizeably smaller baryonic loading of GRB jets.

It is worth highlighting that this analysis accounts for the contribution to the observed diffuse astrophysical neutrino flux of long-resolved GRBs (i.e. triggered). A potentially interesting contribution is constituted by the many GRBs that elude detection (due to their low photon flux) and which is here left unconstrained. As estimated, e.g. by Liu & Wang (2013), the neutrino flux from such unresolved GRBs might even be larger than the one due to resolved ones. In addition to this, other interesting classes of sources possibly contributing to the diffuse astrophysical neutrino flux detected by IceCube are:

- (i) low-luminous GRBs (LLGRBs) (e.g. Murase et al. 2006; Gupta & Zhang 2007), namely GRBs characterized by a luminosity $\lesssim 10^{49}$ erg s⁻¹;
- (ii) choked GRBs, which being opaque to radiation in the GeV–TeV band might show up as neutrino sources hidden with respect to gamma-ray observations (e.g. Meşzafoş & Waxman 2001; Murase & Ioka 2013; Senno, Murase & Meşzafoş 2016).

10 SUMMARY AND CONCLUSIONS

Using ANTARES data from the end of 2007–2017, a search for upward-going muon neutrinos and antineutrinos in spatial and temporal coincidence with 784 GRBs has been performed. The numerical model NeuCosMA was used to estimate the expected neutrino flux from each burst individually, in the context of one-zone internal shock model. A novel aspect of the search here presented is the inclusion in the data analysis chain of the uncertainty that possible unknown parameters, related to the characteristic activity of the central engine, can introduce in the neutrino flux evaluation. This is crucial in order to correctly interpret the validity of model-dependent results, in terms of upper limits set by non-detections of neutrinos in coincidence with GRBs (Adrián-Martínez et al. 2013; Aartsen et al. 2017). These parameters have been identified in the bulk Lorentz factor, variability time-scale, and source redshift, all of which are affecting the so-called dissipation radius, where shell collisions are realized. Among these parameters, the former

was shown to impact the most GRB-neutrino flux predictions. At the same time, it is also possible to marginalize the uncertainty related to it by assuming a correlation with the source isotropic gamma-ray luminosity (which is in turn a physical observable). This was realized by relying upon the observational correlation found by Lü et al. (2012). As a result of such procedure, the minimum variability time-scale was found to contribute more than redshift to the uncertainty on the neutrino flux predictions from GRBs. Indeed, when letting t_v free to vary, the estimated uncertainty on the neutrino flux expected from the model is observed to span up to several orders of magnitude. As a consequence, the expected ν -fluxes are provided with an uncertainty band of $\pm 2\sigma$. Analogously to previous ANTARES searches (Adrián-Martínez et al. 2013, 2017b; Celli et al. 2017), MC simulations of the signal predicted by NeuCosmA were performed, while the respective background was estimated directly from off-source data collected by ANTARES. Only track-like events reconstructed within 10° in radius from the expected GRB position were selected and in temporal correlation with the prompt gamma-ray emission.

The analysis was optimized on a burst-by-burst basis so as to maximize the discovery potential of the search, thus allowing the identification of the most promising GRBs for ANTARES. However, because a negligible reduction of the $MDP_{3\sigma}$ would have been obtained when stacking the entire catalogue, the flux from the whole sample of 784 GRBs was investigated. After unblinding ANTARES data occurred in space and time correlation with GRBs, no event was found to pass the selection criteria, and limits on the contribution of the detected GRB population to the neutrino quasi-diffuse flux were derived. The limits obtained on the cumulative neutrino fluence $E_{\nu_\mu}^2 F_{\nu_\mu}$, relative to the predictions of NeuCosmA, are $1.3_{-0.8}^{+4.1} \times 10^{-2} \text{ GeV cm}^{-2}$ and $0.8_{-0.7}^{+5.2} \times 10^{-1} \text{ GeV cm}^{-2}$, corresponding to $1.3_{-0.8}^{+0.4} \times 10^{-9} \text{ GeV cm}^{-2} \text{ s}^{-1} \text{ sr}^{-1}$ and $1.0_{-0.5}^{+0.9} \times 10^{-8} \text{ GeV cm}^{-2} \text{ s}^{-1} \text{ sr}^{-1}$, respectively, in terms of quasi-diffuse flux $E_{\nu_\mu}^2 \phi_{\nu_\mu}$ in the energy range from $\sim 60 \text{ TeV}$ to $\sim 10 \text{ PeV}$. For the sake of completeness, an upper limit was also calculated relatively to the analysis that assumes the Ghirlanda et al. (2012) correlation as a reference model, and it was found to be at a comparable flux level of the one presented here.

With these results, ANTARES data provide a further and independent constrain on the contribution of GRBs to the astrophysical neutrino flux. In particular, within standard assumptions of energy partition among accelerated hadrons, leptons, and magnetic fields (baryonic loading equal to 10), GRBs are not the main sources of the astrophysical neutrino flux, possibly contributing for less than 10 per cent at energies around 100 TeV.

ACKNOWLEDGEMENTS

The authors acknowledge the financial support of the funding agencies: Centre National de la Recherche Scientifique (CNRS), Commissariat à l'énergie atomique et aux énergies alternatives (CEA), Commission Européenne (FEDER fund and Marie Curie Program), Institut Universitaire de France (IUF), LabEx UnivEarthS (ANR-10-LABX-0023 and ANR-18-IDEX-0001), Région Île-de-France (DIM-ACAV), Région Alsace (contrat CPER), Région Provence-Alpes-Côte d'Azur, Département du Var and Ville de La Seyne-sur-Mer, France; Bundesministerium für Bildung und Forschung (BMBF), Germany; Istituto Nazionale di Fisica Nucleare (INFN), Italy; Nederlandse organisatie voor Wetenschappelijk Onderzoek (NWO), the Netherlands; Council of the President of the Russian Federation for young scientists and leading

scientific schools supporting grants, Russia; Executive Unit for Financing Higher Education, Research, Development and Innovation (UEFISCDI), Romania; Ministerio de Ciencia, Innovación, Investigación y Universidades (MCIU): Programa Estatal de Generación de Conocimiento (refs. PGC2018-096663-B-C41, -A-C42, -B-C43, -B-C44) (MCIU/FEDER), Severo Ochoa Centre of Excellence and MultiDark Consolider (MCIU), Junta de Andalucía (ref. SOMM17/6104/UGR and A-FQM-053-UGR18), Generalitat Valenciana: Grisolia (ref. GRISOLIA/2018/119), Spain; Ministry of Higher Education, Scientific Research and Professional Training, Morocco. We also acknowledge the technical support of Ifremer, AIM and Foselev Marine for the sea operation and the CC-IN2P3 for the computing facilities.

DATA AVAILABILITY

Release and preservation of data used by the ANTARES Collaboration as the basis for publications are guided by the ANTARES policy as written in its Memorandum of Understanding among the collaborating institutions. Part of the data are available on the website: <https://antares.in2p3.fr/publicdata.html> and periodically updated.

REFERENCES

- Aartsen M. G. et al., 2013, *Science*, 342, 1242856
Aartsen M. G. et al., 2014, *Phys. Rev. Lett.*, 113, 101101
Aartsen M. G. et al., 2015a, preprint (arXiv:1510.05223)
Aartsen M. G. et al., 2015b, *ApJ*, 805, L5
Aartsen M. G. et al., 2016, *ApJ*, 824, 115
Aartsen M. G. et al., 2017, *ApJ*, 843, 112
Abbasi R. et al., 2008, *Phys. Rev. Lett.*, 100, 101101
Abdalla H. et al., 2019, *Nature*, 575, 464
Abdo A. A. et al., 2009a, *Nature*, 462, 331
Abdo A. A. et al., 2009b, *Science*, 323, 1688
Abdo A. A. et al., 2009c, *ApJ*, 706, L138
Abraham J. et al., 2010, *Phys. Lett. B*, 685, 239
Acciari V. A. et al., 2019, *Nature*, 575, 455
Ackermann M. et al., 2014, *Science*, 343, 42
Adrián-Martínez S. et al., 2012a, *JINST*, 7,08, T08002
Adrián-Martínez S. et al., 2012b, *ApJ*, 760, 53
Adrián-Martínez S. et al., 2013, *A&A*, 559, A9
Adrián-Martínez S. et al., 2017a, *Eur. Phys. J. C*, 77, 20
Adrián-Martínez S. et al., 2017b, *MNRAS*, 469, 906
Ageron M. et al., 2011, *Nucl. Instr. Meth. A*, 656, 11
Aguilar J. A. et al., 2011, *Astropart. Phys.*, 34, 652
Ahrens J. et al., 2004, *Astropart. Phys.*, 20, 507
Albert A. et al., 2017, *Phys. Rev. D*, 96, 082001
Albert A. et al., 2018, *Eur. Phys. J. C*, 78, 1006
Albert A. et al., 2020, preprint (arXiv:2007.00931)
Aptekar R. et al., 1995, *Space Sci. Rev.*, 71, 265
Asano K., Terasawa S., 2009, *ApJ*, 705, 1714
Atwood W. B. et al., 2009, *ApJ*, 697, 1071
Ajello M. et al., 2019, *ApJ*, 878, 52
Band D. et al., 1993, *ApJ*, 413, 281
Barlow R., 1990, *Nucl. Instr. Meth. A*, 297, 496
Bell A. R., 1978, *MNRAS*, 182, 147
Bhat P. N. et al., 2016, *ApJS*, 223, 28
Blandford R. D., McKee C. F., 1976, *Phys. Fluids*, 19, 1130
Bustamante M., Baerwald P., Murase K., Winter W., 2015, *Nat. Commun.*, 6, 6783
Bustamante M., Heinze J., Murase K., Winter W., 2017, *ApJ*, 837, 33
Celli S. et al., 2017, *Proc. Sci. ICRC*, 301, 988
Chand V. et al., 2020, *ApJ*, 898, 42
Daigle F., Mochkovitch R., 1998, *MNRAS*, 296, 275

- de Naurois M., 2019, *Astron. Telegram*, 13052, 1
- Dornic D., Coleiro A., Colomer-Molla M., Kouchner A., Pradier T., 2019, *Proc. Sci. ICRC*, 358, 872
- Gaisser T. K., Hillas A. M., 1977, *Proc. Sci. ICRC*, 8, 353
- Gehrels N. et al., 2004, *ApJ*, 611, 1005
- Ghirlanda G., Nava L., Ghisellini G., Celotti A., Burlon D., Covino S., Melandri A., 2012, *MNRAS*, 420, 483
- Ghisellini G. et al., 2020, *A&A*, 636, A82
- Globus N., Allard D., Mochkovitch R., Parizot E., 2015, *MNRAS*, 451, 751
- Golkhou V. Z., Butler N. R., 2014, *ApJ*, 787, 90
- Golkhou V. Z., Butler N. R., Littlejohns O. M., 2015, *ApJ*, 811, 93
- Gruber D. et al., 2014, *ApJS*, 211, 12
- Guetta D., Hopper D., Alvarez-Muniz J., Halzen F., Reuveni E., 2004, *Astropart. Phys.*, 20, 429
- Gupta N., Zhang B., 2007, *Astropart. Phys.*, 27, 386
- Gupta N., Zhang B., 2008, *MNRAS*, 384, L11
- He H.-N., Liu R.-Y., Wang X.-Y., Nagataki S., Murase K., Dai Z.-G., 2012, *ApJ*, 752, 29
- Hümmer S., Rieger M., Spanier F., Winter W., 2010, *ApJ*, 721, 630
- Hümmer S., Philipp B., Walter W., 2012, *Phys. Rev. Lett.*, 108, 231101
- Kobayashi S., Piran T., Sari R., 1997, *ApJ*, 490, 92
- Kumar P., McMahon E., 2008, *MNRAS*, 384, 33
- Levan A. J., Cenko S. B., Perley D. A., Tanvir N. R., 2013, *GCN Circular* 14455
- Lithwick Y., Sari R., 2001, *ApJ*, 555, 540
- Liu R.-Y., Wang X.-Y., 2013, *ApJ*, 766, 73
- Lü J., Zou Y. C., Lei W. H., 2012, *ApJ*, 751, 49
- Lyutikov M., 2006, *MNRAS*, 369, L5
- Meegan C. A., Fishman G. J., Wilson R. B., Paciesas W. S., Pendleton G. N., Horack J. M., Brock M. N., Kouveliotou C., 1992, *Nature*, 355, 143
- Meegan C. A. et al., 2009, *ApJ*, 702, 791
- Meşzaős P., 2006, *Rept. Prog. Phys.*, 69, 2259
- Meşzaős P., Rees M. J., 2000, *ApJ*, 530, 292
- Meşzaős P., Waxman E., 2001, *Phys. Rev. Lett.*, 87, 171102
- Milgrom M., Usov V., 1995, *ApJ*, 449, L37
- Murase K., 2008, *Phys. Rev. D*, 78, 101302
- Murase K., Ioka K., 2013, *Phys. Rev. Lett.*, 111, 121102
- Murase K., Nagataki S., 2006, *Phys. Rev. D*, 73, 063002
- Murase K., Ioka K., Nagataki S., Nakamura T., 2006, *ApJ*, 651, L5
- Murase K., Ioka K., Nagataki S., Nakamura T., 2008, *Phys. Rev. D*, 78, 023005
- Murase K., Kashiyama K., Meşzaős P., 2013, *Phys. Rev. Lett.*, 111, 131102
- Paczynski B., 1986, *ApJ*, 308, L43
- Paczynski B., Xu G., 1994, *ApJ*, 427, 708
- Piran T., 1999, *Phys. Rep.*, 314, 575
- Piran T., 2004, *Rev. Mod. Phys.*, 76, 1143
- Rayleigh J. W. S., 1880, *Lond. Edinb. Phil. Mag.*, 10, 73
- Rees M., Meşzaős P., 1992, *MNRAS*, 258, 41
- Sahu S., López Fortín C. E., 2020, *ApJ*, 895, L41
- Sari R., Piran T., 1999, *ApJ*, 520, 641
- Schneider A. et al., 2019, *Proc. Sci. ICRC*, 358, 1004
- Senno N., Murase K., Meşzaős P., 2016, *Phys. Rev. D*, 93, 083003
- Sonbas E., MacLachlan G. A., Dhuga K. S., Veres P., Shenoy A., Ukwatta T. N., 2015, *ApJ*, 805, 86
- Stettner J. et al., 2019, *Proc. Sci. ICRC*, 358, 1017
- Thompson C., 1994, *MNRAS*, 270, 480
- Valeev A. F., Castro-Tirado A. J., Hu Y. D., Garcia E. F., 2019, *GCN Circ.* 25565
- Vietri M., 1995, *ApJ*, 453, 883
- von Kienlin A. et al., 2014, *ApJS*, 211, 13
- Waxman E., 1995, *ApJ*, 452, L1
- Waxman E., Bahcall J., 1997, *Phys. Rev. Lett.*, 78, 2292
- Xu D., Levan A. J., Fynbo J. P. U., Tanvir N. R., D'Elia V., Malesani D., 2014, *GCN Circ.* 16983
- Zatsepin G., Kuzmin V., 1966, *JETP Lett.*, 4, 78
- Zhang B., Kumar P., 2013, *Phys. Rev. Lett.*, 110, 121101
- Zhang B., Kumar P., 2015, *Phys. Rep.*, 561, 1
- Zou Y. C., Piran T., 2010, *MNRAS*, 402, 1854

APPENDIX A: DETERMINING THE BULK LORENTZ FACTOR

The bulk Lorentz factor Γ of the stellar ejecta is a key parameter to understand the physics of GRBs, extremely powerful sources with an intrinsic mildly relativistic nature. In the standard fireball scenario, the temporal evolution of the jet's speed can be approximated as an initial acceleration phase, followed by a period with Γ constant before reaching the external medium and decelerating in it (Zhang & Kumar 2015).

The bulk Lorentz factor determines the frequency of plasma shell collisions and consequently the rate of particle acceleration. Γ affects the shape of neutrino spectra and, in particular, the spectral breaks. The first derivations of the energy breaks were performed by Guetta et al. (2004), who predicted two energy breaks in the neutrino spectra at the energies

$$\epsilon_{\nu,1} \propto (1+z)^{-2} \Gamma_{2.5}^2 \epsilon_{\gamma, \text{MeV}}^{-1} \quad (\text{A1})$$

and

$$\epsilon_{\nu,2} \propto (1+z)^{-1} \Gamma_{2.5}^2 R_{\text{is}} L_{\gamma,52} \epsilon_B^{-1/2}, \quad (\text{A2})$$

where $\Gamma_{2.5} = \Gamma/(10^{2.5})$ and $\epsilon_{\gamma, \text{MeV}} = \epsilon_{\gamma}/\text{MeV}$ is the photon energy. The first break, in equation (A1), is due to the synchrotron break observed in the photon spectrum and the second one, in equation (A2), comes from the onset of cooling losses in high-energy muons. Within the model implemented in NeuCosmA (see Section 4), a third break is expected in the combined $\nu_{\mu} + \bar{\nu}_{\mu}$ spectrum, due to the onset of cooling losses in pions (Hümmer et al. 2012).

The stochastic nature of GRBs, in addition with the complex dynamical evolution of the jet, makes it hard to reliably determine a bulk Lorentz factor. In the previous ANTARES search, as well as in several IceCube searches, a default value of $\Gamma = 316$ was used (Adrián-Martínez et al. 2013). In Fig. A1(a), the stacking fluence obtained in this work is compared with the previous ANTARES estimation, both computed with one-zone modelling of NeuCosmA. However, in this work, a novel method for the estimation of Γ is presented, consisting into exploiting the observed correlation among Γ and the burst's isotropic luminosity, as found by Lü et al. (2012) and reported in equation (2). None the less, such a correlation cannot be used straightforwardly in most of the cases, since it would require the knowledge of the redshift for each GRB of the sample. Unfortunately, redshift is unknown in 90 per cent of the cases: in this situation, for each GRB with z not measured, up to 1000 values of redshift are randomly extracted from a redshift distribution that follows that of long GRBs detected since 2005 by the *Swift* satellite (see Fig. 2). Then, from such 1000 values of z , 1000 values of bulk Lorentz factor are calculated through equation (2). By averaging the resulting 1000 values of Γ for an individual GRB, $\langle \Gamma \rangle$ is obtained. The resulting cumulative neutrino fluence is shown in Fig. A2(a), where it is also compared with the expected neutrino fluence estimated by the previous ANTARES analysis (Adrián-Martínez et al. 2013). The two are observed at a comparable level, even though the latest analysis has more than twice more sources than the previous. This result is in fact a consequence of the neutrino modelling adopted: while past predictions tended to overestimate the expected flux by assuming standard values for model parameters, here an accurate modelling is realized by accounting for variations in these parameters reflecting the properties of observed GRBs. An example is given in Fig. A2(b), where the distribution of the $\langle \Gamma \rangle$ values obtained for each burst is shown and compared with the standard value used in the past. The obtained distribution peaks at a value lower than $\Gamma = 316$.

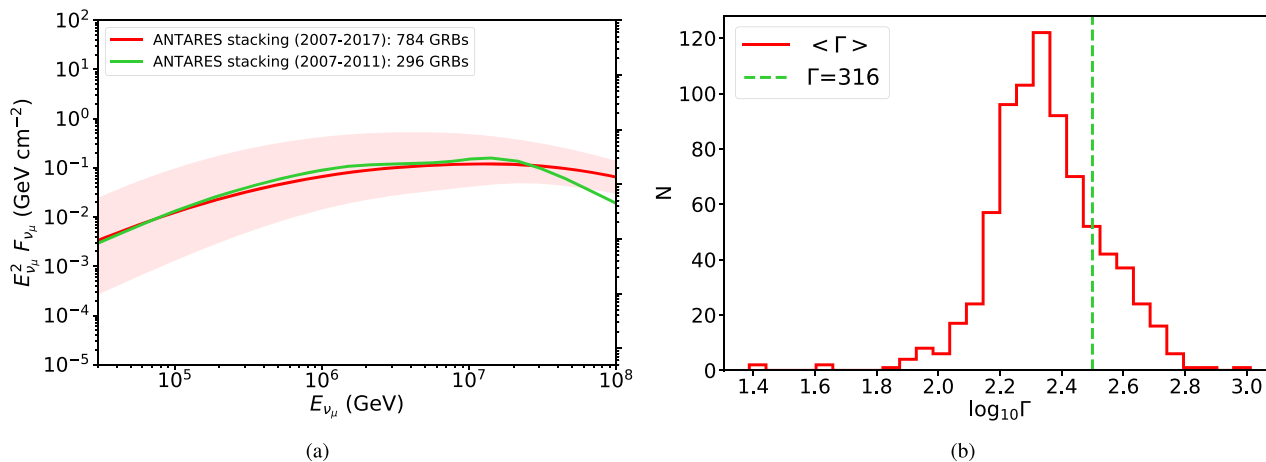


Figure A1. (a) Comparison between the cumulative neutrino fluence expected from the stacking of 784 GRBs in the period 2007–2017 (in red) and the cumulative neutrino fluence obtained in Adrián-Martínez et al. (2013) from stacking 296 GRBs in the years 2007–2011 (in green). The red shaded region indicates the error band around the neutrino fluence estimated in this work, taking into account the several uncertainties affecting the neutrino production in GRBs. (b) Logarithmic distribution of the average bulk Lorentz factor ($\langle \Gamma \rangle$) for any burst in the sample (in red), in comparison with default value $\Gamma = 316$ (dashed green line) previously used by Adrián-Martínez et al. (2013). Note that, whenever a measurement of z is missing, (Γ) is obtained by averaging the 1000 values of redshift extracted for each GRB. On the other hand, for GRBs with measured z , a single contribution of Γ is present in this plot, as given by equation (2).

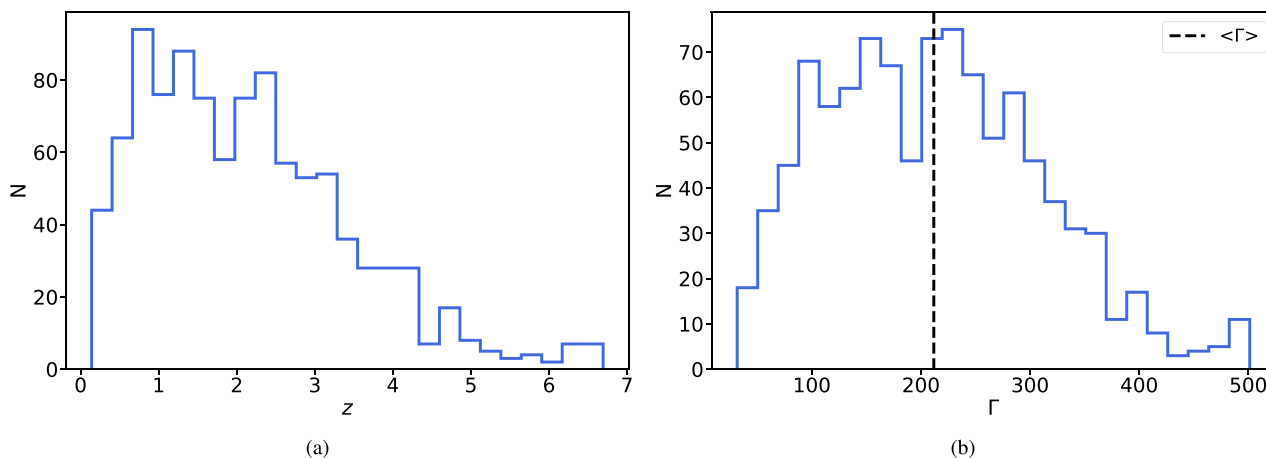


Figure A2. (a) Distributions of the redshift z values randomly extracted for GRB08102853. (b) Corresponding bulk Lorentz factor Γ values obtained by using the correlation in equation (2) (Lü et al. 2012). The black dashed line shows the average Γ of the considered GRB, ($\langle \Gamma \rangle \simeq 210$).

An example of the procedure just explained is shown for GRB08102853 in Figs A2(a) and (b), where the redshift and subsequent Lorentz factor distributions are shown, respectively.

Moreover, it is worth to recall that in this work measured values of the minimum variability time-scale are also used when available, or they are extracted from a distribution of known values. This is another difference with respect to what was assumed in the previous ANTARES search where $t_v = 10$ ms was considered for all GRBs irrespective of their actual light curve. These differences do have an impact, as shown in this work, on the neutrino spectral shape in comparison with previous analyses.

APPENDIX B: INDIVIDUAL NEUTRINO FLUENCE SIMULATIONS

In this appendix, the uncertainty due to missing parameters on individual GRB-neutrino fluences is explored, as explained in Section 4,

and few examples of neutrino spectra obtained with NeuCosMA are reported. The unknown parameters investigated here are the redshift z and the minimum variability time-scale t_v only, as the uncertainty on the bulk Lorentz factor is marginalized by assuming Γ values satisfying the correlation given in equation (2). The goal is hence to derive which among these parameters most affects the neutrino flux computation.

Several cases are shown, covering all the parameter combinations realized in the selected GRB sample, namely (i) GRB08021273, a source with both z and t_v unknown (Fig. B1a); (ii) GRB14102845, a source with measured $z = 2.332$ but t_v unknown (Fig. B1b); (iii) GRB08102853, a source with z unknown and $t_v = 0.35$ s measured (Fig. B1c); (iv) GRB13042732 (also known as GRB130427A), the brightest ever detected GRB in gamma rays, for which both $z = 0.34$ and $t_v = 0.04$ s are measured (Fig. B1d).

For each of these GRBs, 1000 simulations are performed extracting the unknown value of the missing parameter, either the redshift or the variability time, from a distribution of the same parameter

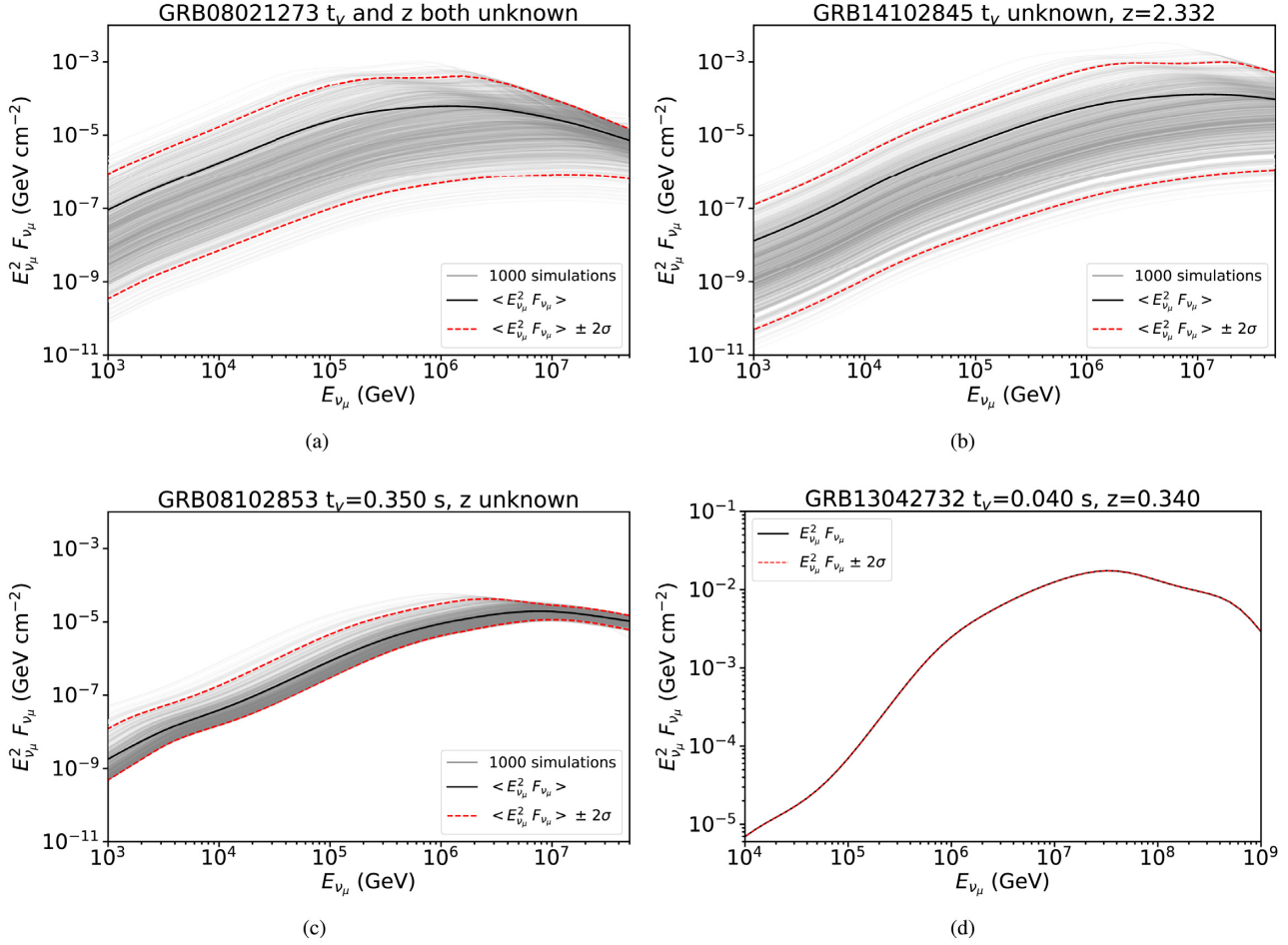


Figure B1. Expected neutrino fluence $E_{\nu_\mu}^2 F_{\nu_\mu}$ as a function of the neutrino energy E_{ν_μ} . The z and t_ν values of each GRB are indicated in the panels, when known: (a) GRB08021273; (b) GRB14102845 (Xu et al. 2014); (c) GRB08102853 (Golkhou et al. 2015); and (d) GRB13042732 (Levan et al. 2013; Sonbas et al. 2015). The grey thin lines indicate the results of 1000 simulations performed with the several randomly extracted values of z and t_ν , when at least one of such parameters is unknown. The black thick line shows the mean of all the simulations or, when both z and t_ν are known, the resulting neutrino fluence. The red dashed lines delineate the error band around the neutrino fluence. In case both the minimum variability time-scale and the redshift are fixed, as for the GRB shown in (d), the fluence uncertainty is extremely tiny: in this particular case, e.g. it is estimated to be ~ 3 per cent.

as obtained from other known GRBs. From these examples, it follows that the minimum variability time-scale contributes to the uncertainty on the neutrino fluence expected from GRBs significantly more than redshift. In fact, by comparing the cases (ii) and (iii) in Figs B1(b) and (c), respectively, it is possible to note that the uncertainty due to the unknown value of z is contained within ~ 1 order of magnitude with respect to the mean flux, while it spans over several orders of magnitude when t_ν is unknown. On the other hand, when both z and t_ν are measured, the error band on the neutrino flux is extremely reduced, as it is only due to the uncertainty in the measurements of spectral parameters. In these cases, it is not possible to distinguish the upper and lower bounds on the neutrino fluence from the mean fluence: an example is shown in Fig. B1(d) for GRB13042732.

So far, the uncertainty related to the knowledge on Γ was not considered, as justified by the assumption of a correlation that allows to infer its value, once the isotropic gamma-ray luminosity of the burst is given. The effects related to considering a different correlation are investigated in Appendix C.

APPENDIX C: EVALUATING SYSTEMATICS ON NEUTRINO FLUXES

In addition to the parameter uncertainties considered so far, namely those due to the poor knowledge of redshift and minimum variability time-scale (see Section 4.2 and Appendix B), a further major source of uncertainty is related to the systematics on the treatment of the Lorentz factor, which could significantly affect the neutrino expectation from GRBs (He et al. 2012). In fact, the present analysis relies upon the correlation between the isotropic gamma-ray luminosity $L_{\gamma, \text{iso}}$ and Γ as derived by Lü et al. (2012), which has allowed the values of bulk Lorentz factor for each GRB in the sample to be determined by using equation (2), as explained in details in Appendix A.

In order to evaluate the impact of such a method on neutrino expectations, the correlation found by Ghirlanda et al. (2012) was also tested. The latter one actually relates Γ to the peak gamma-ray luminosity $L_{\gamma, \text{peak}}$. Hence, as an intermediate step, the Ghirlanda et al. (2012) data sample was re-analysed to obtain the corresponding relation between Γ and isotropic gamma-ray luminosity $L_{\gamma, \text{iso}}$,

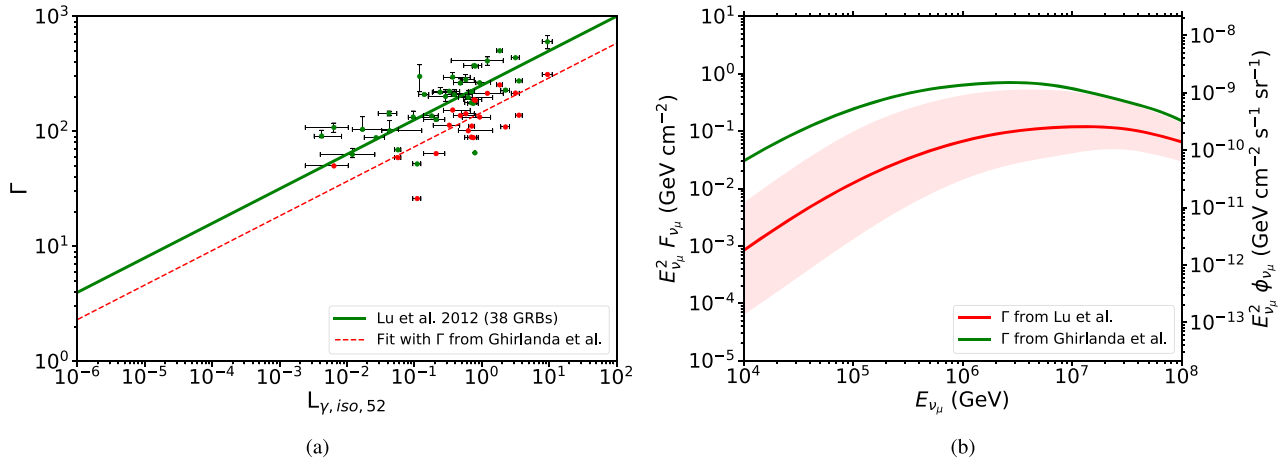


Figure C1. (a) The bulk Lorentz factor Γ as a function of the isotropic equivalent gamma-ray luminosity $L_{\gamma, \text{iso}}$. The green points represent GRBs in the sample studied by Lü et al. (2012). The red points, instead, are a subsample of the Ghirlanda et al. (2012) sample, containing only those GRBs in common with Lü et al. (2012), such that the values of Γ come from Ghirlanda et al. (2012), while the corresponding values of $L_{\gamma, \text{iso}}$ are from Lü et al. (2012). The green solid and dashed red lines represent the best fits of each sample. (b) Total neutrino fluence $E_{\nu\mu}^2 F_{\nu\mu}$ expected from the 784 GRBs in the ANTARES 2007–2017 sample (left-hand axis) and corresponding quasi-diffuse neutrino flux $E_{\nu\mu}^2 \phi_{\nu\mu}$ (right-hand axis). The red and green lines show the different results obtained by assuming a Γ -distribution either according to Lü et al. (2012) [see equation (2)] or according to Ghirlanda et al. (2012) [see equation (C1)], respectively. The red shaded region indicates the error band around the stacking flux expected from Lü et al. (2012), as estimated in Section 4.3.

similarly to the equation (2). Only common GRBs with respect to Lü et al. (2012) were selected from the Ghirlanda et al. (2012) GRB sample, in order to consider the Γ estimation from Ghirlanda et al. (2012) and the corresponding $L_{\gamma, \text{iso}}$ from Lü et al. (2012). From this sample, the following correlation was found:

$$\Gamma_G \simeq 146 L_{\gamma, \text{iso}, 52}^{0.30} \quad (\text{C1})$$

The comparison among such a correlation and the one obtained by Lü et al. (2012) is shown in Fig. C1(a). As visible, the Lorentz factor values obtained by Ghirlanda et al. (2012) are systematically lower by a factor of ~ 2 with respect to the values obtained by Lü et al. (2012). To quantify the impact of considering a reduced Lorentz factor on the expected number of neutrino events, the same method described in Section 4.2 was applied to the computation of neutrino spectra, namely for each GRB in the sample, 1000 spectral simulations were performed with NeuCosmA by extracting Γ according to equation (C1). By summing over all 784 GRBs, a revised stacking flux was obtained, as shown in Fig. C1(b). The spectral normalization appears now significantly higher with respect to the scenario described in Section 4.3, while the peak energy of the neutrino spectrum is shifted towards lower energies.

With this novel neutrino spectrum, it is possible to re-run the data analysis chain by optimizing the track-quality cut Λ_{cut} consistently with the procedure described in Section 8. Interestingly, the resulting cuts are found unaffected for most of the GRB sample. None the less, the increased neutrino flux derived by adopting the Ghirlanda et al. (2012) method to estimate the bulk Lorentz factor implies a higher number of expected events in ANTARES with respect to the computation derived in Section 9 for the correlation by Lü et al. (2012). In particular, this is estimated to be $n_s \simeq 0.36$, which is more than a factor of 10 above the estimate presented in equation (7). From the comparison with the estimated uncertainty due to missing information on redshift and variability time-scale, which is contained within a factor of ~ 5 (2σ), it is possible to conclude that the leading source of uncertainty in neutrino spectral modelling is represented by the indirect knowledge of the bulk Lorentz factor of GRB jets.

This conclusion is also supported by recent studies from He et al. (2012).

¹Université de Strasbourg, CNRS, IPHC UMR 7178, F-67000 Strasbourg, France

²Université de Haute Alsace, F-68200 Mulhouse, France

³Technical University of Catalonia, Laboratory of Applied Bioacoustics, Rambla Exposició, E-08800 Vilanova i la Geltrú, Barcelona, Spain

⁴INFN, Sezione di Genova, Via Dodecaneso 33, I-16146 Genova, Italy

⁵Friedrich-Alexander-Universität Erlangen-Nürnberg, Erlangen Centre for Astroparticle Physics, Erwin-Rommel-Str. 1, D-91058 Erlangen, Germany

⁶Institut d'Investigació per a la Gestió Integrada de les Zones Costaneres (IGIC) - Universitat Politècnica de València. C/Paraninf 1, E-46730 Gandia, Spain

⁷Aix Marseille Univ, CNRS/IN2P3, CPPM, Marseille, France

⁸Université de Paris, CNRS, Astroparticule et Cosmologie, F-75013 Paris, France

⁹Aix Marseille Univ, CNRS, CNES, LAM, Marseille, France

¹⁰National Center for Energy Sciences and Nuclear Techniques, B.P.1382, R. P.10001 Rabat, Morocco

¹¹INFN, Laboratori Nazionali del Sud (LNS), Via S. Sofia 62, I-95123 Catania, Italy

¹²University Mohammed V in Rabat, Faculty of Sciences, 4 av. Ibn Battouta, B.P. 1014, R.P. 10000 Rabat, Morocco

¹³University Mohammed I, Laboratory of Physics of Matter and Radiations, B.P.717, Oujda 6000, Morocco

¹⁴Nikhef, Science Park, Amsterdam, the Netherlands

¹⁵Institute of Space Science, RO-077125 Bucharest, Măgurele, Romania

¹⁶Universiteit van Amsterdam, Instituut voor Hoge-Energie Fysica, Science Park 105, NL-1098 XG Amsterdam, the Netherlands

¹⁷INFN, Sezione di Roma, P.le Aldo Moro 2, I-00185 Roma, Italy

¹⁸Dipartimento di Fisica dell'Università La Sapienza, P.le Aldo Moro 2, I-00185 Roma, Italy

¹⁹LPHEA, Faculty of Science, Semaili, Cadi Ayyad University, P.O.B. 2390, Marrakech, Morocco

²⁰INFN, Sezione di Bologna, Viale Berti-Pichat 6/2, I-40127 Bologna, Italy

²¹INFN, Sezione di Bari, Via E. Orabona 4, I-70126 Bari, Italy

²²IFIC, Instituto de Física Corpuscular (CSIC – Universitat de València) c/ Catedrático José Beltrán, 2 E-46980 Paterna, Valencia, Spain

²³*Department of Computer Architecture and Technology/CITIC, University of Granada, E-18071 Granada, Spain*

²⁴*Géozur, UCA, CNRS, IRD, Observatoire de la Côte d'Azur, Sophia Antipolis, France*

²⁵*Dipartimento di Fisica dell'Università, Via Dodecaneso 33, I-16146 Genova, Italy*

²⁶*Université Paris-Sud, F-91405 Orsay Cedex, France*

²⁷*Dipartimento di Fisica e Astronomia dell'Università, Viale Berti Pichat 6/2, I-40127 Bologna, Italy*

²⁸*Laboratoire de Physique Corpusculaire, Clermont Université, Université Blaise Pascal, CNRS/IN2P3, BP 10448, F-63000 Clermont-Ferrand, France*

²⁹*LIS, UMR Université de Toulon, Aix Marseille Université, CNRS, F-83041 Toulon, France*

³⁰*Royal Netherlands Institute for Sea Research (NIOZ) and Utrecht University, Landsdiep 4, NL-1797 SZ 't Horntje (Texel), the Netherlands*

³¹*International Centre for Radio Astronomy Research, Curtin University, Bentley, WA 6102, Australia*

³²*Huygens–Kamerlingh Onnes Laboratorium, Universiteit Leiden, the Netherlands*

³³*Institut für Theoretische Physik und Astrophysik, Universität Würzburg, Emil-Fischer Str. 31, D-97074 Würzburg, Germany*

³⁴*Institut Universitaire de France, F-75005 Paris, France*

³⁵*Dr. Remeis-Sternwarte and ECAP, Friedrich-Alexander-Universität Erlangen-Nürnberg, Sternwartstr. 7, D-96049 Bamberg, Germany*

³⁶*Moscow State University, Skobeltsyn Institute of Nuclear Physics, Leninskie gory, 119991 Moscow, Russia*

³⁷*Mediterranean Institute of Oceanography (MIO), Aix-Marseille University, F-13288, Marseille, Cedex 9, France; Université du Sud Toulon-Var, CNRS-INSU/IRD UM 110, F-83957, La Garde Cedex, France*

³⁸*INFN, Sezione di Catania, Via S. Sofia 64, I-95123 Catania, Italy*

³⁹*Dpto. de Física Teórica y del Cosmos & C.A.F.P.E., University of Granada, E-18071 Granada, Spain*

⁴⁰*IRFU, CEA, Université Paris-Saclay, F-91191 Gif-sur-Yvette, France*

⁴¹*INFN, Sezione di Napoli, Via Cintia, I-80126, Napoli, Italy*

⁴²*Museo Storico della Fisica e Centro Studi e Ricerche Enrico Fermi, Piazza del Viminale 1, I-00184 Rome, Italy*

⁴³*INFN-CNAF, Viale C. Berti Pichat 6/2, I-40127, Bologna, Italy*

⁴⁴*Dipartimento di Fisica dell'Università Federico II di Napoli, Via Cintia, I-80126, Napoli, Italy*

This paper has been typeset from a $\text{\TeX}/\text{\LaTeX}$ file prepared by the author.